Connection between magnetism and structure in Fe double chains on the Ir(100) surface

Riccardo Mazzarello[1,*] and Erio Tosatti[1,2]
[1]*SISSA, Via Beirut 2/4, 34014 Trieste, Italy and DEMOCRITOS-INFM, Via Beirut 2/4, 34014 Trieste, Italy*
[2]*ICTP, Strada Costiera 11, 34014 Trieste, Italy*

(Received 14 January 2009; revised manuscript received 9 March 2009; published 3 April 2009)

The magnetic ground state of nanosized systems such as Fe double chains, chains recently shown to form in the early stages of Fe deposition on Ir(100), is generally nontrivial. Using *ab initio* density functional theory we find that the straight ferromagnetic (FM) state typical of bulk Fe as well as of isolated Fe chains and double chains is disfavored after deposition on Ir(100) for all the experimentally relevant double chain structures considered. So long as spin-orbit coupling (SOC) is neglected, the double chain lowest energy state is generally antiferromagnetic (AFM), a state which appears to prevail over the FM state due to Fe-Ir hybridization. Successive inclusion of SOC adds two further elements, namely, a magnetocrystalline anisotropy and a Dzyaloshinskii-Moriya (DM) spin-spin interaction; the former stabilizing the collinear AFM state and the latter favoring a long-period spin modulation. We find that anisotropy is most important when the double chain is adsorbed on the partially deconstructed Ir(100)—a state which we find to be substantially lower in energy than any reconstructed structure—so that in this case the Fe double chain should remain collinear AFM. Alternatively, when the same Fe double chain is adsorbed in a metastable state onto the (5×1) fully reconstructed Ir(100) surface, the FM-AFM energy difference is very much reduced and the DM interaction is expected to prevail, probably yielding a helical spin structure.

DOI: 10.1103/PhysRevB.79.134402 PACS number(s): 71.70.Ej, 73.20.At, 75.70.Rf, 79.60.Bm

I. INTRODUCTION

Controlling the magnetic order of materials is a long-standing goal of applied solid-state physics, with a tremendous impact on the information technology industry. The onset of a magnetic moment in a transition-metal atom arises primarily out of intra-atomic Hund's rules, which are poorly structure dependent even in a solid. Interatomic magnetic order, however, depends very critically on structure. As is well known, for example, bcc Fe is a prototypical ferromagnetic metal, but the magnetic properties do change with the crystal structure and the Fe-Fe interatomic distance, so that bulk Fe can support antiferromagnetic (AFM) configurations in the metastable fcc structure.[1–5] Low-dimensional and mesoscopic systems offer new possibilities to control the magnetic order of Fe. In particular, the heteroepitaxial growth of Fe films and nanowires on nonmagnetic transition-metal substrates is expected to yield novel magnetic structures due to the combined effects of (a) lattice mismatch, (b) reduced dimensionality, (c) hybridization of Fe *d* orbitals with the substrate, and (d) spin-orbit related effects for heavy metal substrates.

Novel experimental techniques have been developed, such as spin-polarized scanning tunneling microscopy (SP-STM),[6] capable of resolving the magnetic structure of nanosized systems at the atomic level. This technique has recently shown that the ground state of a single monolayer (ML) of Fe on W(001) is a collinear AFM state rather than a ferromagnetic (FM) one.[7] One way to partly rationalize the demise of ferromagnetism in this system could be the observation that the density of states (DOS) at the Fermi energy $n(E_F)$ is strongly depressed upon adsorption.[7] Since the FM susceptibility is essentially proportional to $n(E_F)$, while the AFM susceptibility is not, antiferromagnetism might happen to suffer less from interaction with the substrate and prevail over ferromagnetism because of that. This hypothetical possibility fits the additional experimental observation that Fe monolayers remain FM on W(110), where adsorption is weaker; this different tungsten face being better packed and less reactive than W(001).[8] Single MLs of Fe on Ir(111) have also been shown to be AFM and to form complex, collinear mosaic structures.[9]

Here we are concerned with deposited Fe nanostructures rather than monolayers. The initial steps of Fe deposition on the (1×5) reconstructed Ir(100) surface of Ref. 10 showed that Fe deposition initially forms metastable double chains, which appear to occupy the troughlike double minima of the quasihexagonal Ir(100) top layer height profile. While the presence of the (1×5) periodicity suggests the permanence of reconstruction or at least some amount of reconstruction, it does not actually certify that the pristine quasihexagonal reconstruction of the Ir(100) substrate remains unaltered upon Fe adsorption. The existing data do not permit to resolve the detailed structure of the underlying Ir substrate.[10] The Fe double chains might deposit without altering the initial reconstruction or they may alter it to some extent. Indeed, it is found that the (1×5)Ir(100) reconstruction becomes eventually lifted at high Fe coverage and/or high temperature.[10]

The scope of the present calculations is to analyze and possibly predict the magnetic state of Fe double chains adsorbed on Ir(100). As an added bonus, we wish to establish whether something can be learned from the relationship between magnetism and structure, also in view of the ongoing SP-STM experiments on these systems at low temperatures.[11]

This is not the first theory work on Fe double chains on Ir(100). In Ref. 12 the structure and energetics of this system were already investigated by first-principles density functional theory (DFT). Different adsorption sites were considered and structural relaxations were performed for both FM

and nonmagnetic (NM) configurations. The FM configuration was shown to be always preferred over the NM one, which is consistent with Fe's strong Hund's rule intra-atomic parameters. However, these studies did not examine other interesting possibilities such as AFM or noncollinear orderings. Furthermore the effects of spin-orbit coupling (SOC) were not considered so that no specific easy magnetization axis and magnetocrystalline anisotropy parameters were established.

We will present here two sets of calculations. The first set will investigate collinear spin structures only and, for that purpose, we will use a realistic model of the substrate consisting of a seven-Ir-layer slab. The ground-state energy and optimal state of magnetization of free standing and Ir(100) deposited Fe double chains will be compared without SOC, i.e., within the scalar-relativistic approximation. Here only two possible magnetization states are considered, namely, FM and AFM (same magnetization signs of two Fe atoms across the double chain, alternating signs between first neighbors parallel to the chains). Crucially, different structures will be considered for the underlying Ir(100) substrate and their relative energetics compared. In a second set of calculations, the SOC will be included by switching to the more time-consuming fully relativistic approximation and here different AFM spin directions will be considered, so as to extract magnetic anisotropy energies (MAEs). For MAE calculations the same realistic seven-Ir-layer slab will be used to model the surface. Noncollinear spin structures with opposite chirality will also be considered, so as to extract the Dzyaloshinskii-Moriya (DM) coupling energy. However, because of the larger supercells required along the chain direction to model spin spirals, this set of calculations is limited by computer time economy to smaller and simpler slabs. Eventually, a fairly complete scenario of the structures, energies, and magnetization geometries will emerge, allowing a discussion, and a tentative prediction subject to our rather limited accuracy, of the relationship between them. Our tentative conclusion is that Fe double chains metastably deposited on fully reconstructed Ir(100) may develop long-pitched helical spin structures whereas the same double chains on the partly reconstructed surface, a state of much lower energy, should exhibit a simple, collinear AFM ground state.

II. COMPUTATIONAL METHODS

Standard DFT electronic structure calculations were carried out within a generalized gradient approximation (GGA) with a Perdew-Burke-Ernzerhof (PBE) exchange-correlation functional,[13] as implemented in the plane-wave PWSCF code included in the QUANTUM-ESPRESSO package.[14,15] We employed ultrasoft pseudopotentials generated according to the Rappe-Rabe-Kaxiras-Joannopoulos scheme.[16] The wave functions were expanded in plane waves with a kinetic-energy cutoff of 30 Ry, whereas the charge-density cutoff was 300 Ry for slab calculations and 800 Ry for free-standing wires. In all the structural optimization runs, Hellmann-Feynman forces were calculated with high accuracy (at each step, the allowed error in the total energy was set to 10^{-7} Ry) and a stringent convergence criterion was used for structural energy minimization (all components of all forces required to be smaller than 10^{-3} a.u. and the change in the total energy between two consecutive steps required to be less than 10^{-4} a.u.). Convergence with respect to k points, smearing parameters, wave function, and density cutoff was checked very carefully. Furthermore, the total energies and forces of the optimized structures were recalculated within the projector-augmented wave (PAW) method (same method used in Ref. 12), very recently implemented in the PWSCF code, and found to be in good agreement with the ultrasoft pseudopotential calculations. Free-standing single and double Fe wires in the initial test calculations were modeled by chains parallel to the $\hat{z}$ axis and periodically repeated along the x and y directions. The minimum distance between periodic images was 20 a.u. For single chains, the intrachain spacing was allowed to vary so as to determine the equilibrium spacing. For double chains, the intrachain spacing was set at 2.758 Å, corresponding to the substrate-imposed intrachain spacing of deposited chains which we will need to adopt in later calculations.

The reconstructed Ir(100) surface has (1×5) periodicity and a ~20% higher lateral density (in its quasihexagonal top layer) than a regular bulk (100) plane with its square lattice. A (1×5) supercell was used for the clean Ir(100) and for FM Fe double chains on Ir(100), whereas a (2×5) supercell was required for the AFM case. In the following, the $\hat{y}$ axis will be taken perpendicular to the surface, the $\hat{z}$ axis parallel to the chains, and the $\hat{x}$ axis in the plane and normal to the chains. In all scalar-relativistic calculations and in the SO calculations of magnetic anisotropy, the Ir substrate was modeled as a seven-layer slab periodically repeated across 13 Å wide vacuum regions. Fe double chains were deposited on one face of the slab, while the other face was a perfect (100) surface. Both the reconstruction of the clean surface and the relaxation of Fe/Ir(100) systems were treated by allowing the four topmost Ir layers to relax and starting from a six-atom/cell Ir topmost layer. A few scalar-relativistic test calculations were repeated with a nine-layer symmetric slab with Fe double chains on both faces of the slab. The agreement between these calculations and those carried out with asymmetric seven-layer slabs was very good. A $2\times10\times1$ Monkhorst-Pack mesh[17] of special points was used for the integration over the Brillouin Zone for the (1×5) cell and an equivalent mesh was used for the (2×5) cell. The Fermi function smearing approach of Ref. 18 was used to deal with electron occupancy near the Fermi level, with a smearing parameter of 0.01 Ry. As a test of our pseudopotential, we calculated the lattice parameter, a_0, and the bulk modulus B of bulk fcc Ir. Our results, $a_0=3.90$ Å and $B=3.42$ Mbar, compare very well to the experimental values, $a_0=3.84$ Å and $B=3.55$ Mbar.

III. RESULTS: STRUCTURE

We started off with ideal, free-standing Fe single chains. Similar to previous work,[19–21] we found first of all that the lowest energy state of free-standing Fe chains is FM. In Table I the calculated equilibrium Fe-Fe distance and the magnetization per Fe atom of NM, FM, and AFM chains are

TABLE I. Equilibrium Fe-Fe distance a_0 and magnetization per atom m for FM and AFM free-standing single wires: comparison between our results and recent results. All results in this table were obtained by using GGA functionals.

	Our work		Ref. 19		Ref. 20		Ref. 21	
	a_0 (Å)	m (μ_B)	a_0 (Å)	m (μ_B)	a_0 (Å)	m (μ_B)	a_0 (Å)	m (μ_B)
FM	2.28	3.32	2.25	3.34	2.28	2.98	2.25	3.41
AFM	2.40	3.14	2.38	3.05			2.15	1.82
NM	1.91	0.00	1.94	0.00			1.94	0.0

compared to those given in the literature. The calculated total energy of free single chains in the FM and AFM configuration as a function of Fe-Fe distance is shown in Fig. 1. The epitaxial Fe chains on Ir(100) are stretched lengthwise and the energy difference between AFM and FM chains, $\Delta E = E_{\mathrm{AFM}} - E_{\mathrm{FM}}$, shrinks for stretched wires. At the theoretical intrachain Fe-Fe distance of wires deposited on Ir(100), 2.758 Å, $\Delta E = 0.142$ eV/Fe atom.

For double chains, we restricted ourselves to the 2.758 Å intrachain Fe-Fe distance only. It was found that free-standing Fe double chains are also FM, although the energy difference per Fe atom between FM and AFM is smaller than for isolated chains. Energies and magnetizations of Fe atoms are shown in Table II. The magnetization of an atom is conventionally calculated by integrating the up-down spin density difference in a sphere centered on the atom, with radius equal to half the distance between the atom and its nearest neighbor.

Separately we considered the clean, reconstructed (1×5)Ir(100) surface. The calculated surface energy E_s and work function W of the surface are 1.31 and 5.51 eV, respectively, in excellent agreement with experiments[22,23] and with previous theoretical work.[12,24] The calculated surface energy difference between the perfect (1×1) and the reconstructed (1×5) surface was 0.05 eV/((1×1) area), which also compares well to previous GGA calculations.[24] Note that, had we used the local-density approximation (LDA), the (1×5) reconstructed phase would instead have been unstable,[24] in contrast to experiments.

The structural parameters of the reconstructed Ir(100) surface are shown in Table III (the notation of Ref. 12 is used).

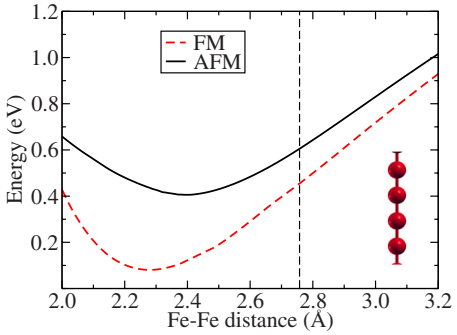

FIG. 1. (Color online) Total energy per atom of FM and AFM free-standing Fe single chains as a function of Fe-Fe distance. Dashed vertical line corresponds to the theoretical interatomic distance of the Fe chain deposited on Ir(100).

Our results are in good agreement with experimental structure parameters as measured by low-energy electron diffraction (LEED) (Ref. 25) as well as with previous calculations.[12,24]

All basic ingredients ready, we proceeded to investigate the properties and energetics of Fe double chains deposited on the Ir substrate. There are three different energy scales at play in this system. The first is the structural scale, involving energy differences of the order of 100 meV/Fe atom. The second is the magnetic intersite exchange scale, involving differences of the order of 10 meV/Fe atom. The third is the spin orientational scale (spin orbit related), involving differences of the order of 1 meV/Fe atom. We stress that the size of intersite exchange interactions between magnetic Fe atoms is 2 orders of magnitude smaller than the intra-atomic "magnetic" exchange energy scale, of order of 1 eV/Fe atom,

TABLE II. Calculated energy differences per atom, ΔE, and magnetizations per atom, m, for NM, FM, and AFM free-standing single chains (SC) and NM, FM, and AFM double chains at interchain distances d_{inter} of 2.33, 2.40, 2.52, and 4.14 Å (corresponding to the interchain distances of Fe double chains in the C_2, C_1, DEC, and C_4 configurations, respectively). The intrachain Fe-Fe distance is 2.758 Å for all the structures. For each structure, ΔE is given with respect to the preferred FM solution. For double chains the interaction energy between chains, E_{int}, is shown as well.

d_{inter} (Å)	Magnetic struct.	ΔE (eV)	E_{int} (eV)	m (μ_B)
(SC)	FM	0.000		3.45
	AFM	0.142		3.38
	NM	2.228		0.00
2.33	FM	0.000	0.835	3.14
	AFM	0.070	0.907	3.16
	NM	1.544	1.519	0.00
2.40	FM	0.000	0.803	3.18
	AFM	0.092	0.854	3.21
	NM	1.631	1.400	0.00
2.52	FM	0.000	0.733	3.25
	AFM	0.116	0.759	3.29
	NM	1.748	1.212	0.00
4.14	FM	0.000	0.083	3.43
	AFM	0.090	0.136	3.37
	NM	2.211	0.101	0.00

TABLE III. Calculated and experimental structural parameters (in angstrom) of the reconstructed Ir(100) surface. The notations defined in Fig. 1 of Ref. 12 are used: d_0 is the bulk interlayer distance, d_{ij} and $\langle d_{ij} \rangle$ are the shortest and average distances between layer i and j, and b_i^{kl} and p_i^k are vertical and lateral displacement amplitudes of atoms k and l in layer i.

	Present Work	LEED	Ref. 12	Ref. 24
d_0	1.95	1.920	1.943	1.916
d_{12}	1.96	1.94	2.00	1.97
$\langle d_{12} \rangle$	2.26	2.25	2.25	
b_1^{13}	0.22	0.25	0.20	
b_1^{23}	0.54	0.55	0.47	0.47
b_1^{34}	−0.21	−0.20	−0.17	−0.20
p_1^2	−0.04	−0.05	−0.03	−0.05
p_1^3	−0.07	−0.07	−0.07	−0.03
d_{23}	1.83	1.79	1.85	1.92
$\langle d_{23} \rangle$	1.91	1.88	1.89	
b_2^{13}	0.05	0.07	0.03	
b_2^{23}	0.10	0.10	0.05	
p_2^2	0.03	0.01	0.00	
p_2^3	0.01	0.02	0.01	
d_{34}	1.88	1.83	1.91	
$\langle d_{34} \rangle$	1.96	1.93	1.96	
b_3^{13}	0.08	0.10	0.05	
b_3^{23}	0.04	0.05	0.02	
p_3^1	−0.01		0.01	
p_3^2	0.00		0.00	
d_{45}	1.94	1.89	1.92	
$\langle d_{45} \rangle$	1.96	1.91	1.93	
b_4^{13}	0.05	0.06	0.03	
b_4^{23}	0.02	0.03	0.01	
p_4^2	0.00		−0.01	
p_4^3	−0.01		−0.01	

due to the very strong Hund's rule intra-atomic interactions.

We proceeded to examine structures first. Several configurations of Fe double wires on Ir(100) were considered, corresponding to different adsorption sites for the Fe atoms (see Fig. 2). Adopting the notation of Ref. 12 we considered C_1, C_2, and C_4 configurations. Configurations C_1 and C_4 correspond to Fe chains adsorbed on the troughs of (1×5)Ir(100), whereas C_2 corresponds to Fe chains sitting on the hills of (1×5)Ir(100). The zig-zag-shaped configuration denoted as C_3 in Ref. 12 was not considered, for scanning tunneling microscopy (STM) images fail to suggest zig-zag-shaped chains.[10]

We found, interestingly, that C_1, C_2, and C_4 configurations were all metastable. This is because the Fe chains should lift the reconstruction of Ir(100) rather than adsorb on the (1×5) fully reconstructed structure. In fact the calculated adsorption energy of double chains on perfect, unreconstructed (1×1)Ir(100), where the top layer is a square lattice, is 0.57 eV/Fe atom larger than on (1×5)Ir(100), where the top layer is a distorted triangular lattice. This energy difference was

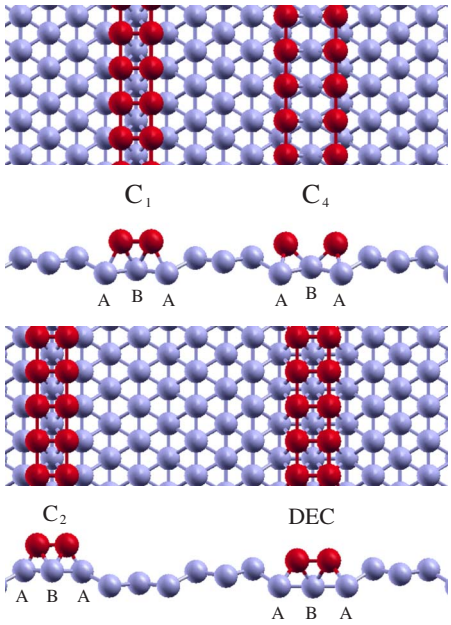

FIG. 2. (Color online) Top and side views of the reconstructed Ir(100) surface with the studied configurations for the dimer chain. Configurations C_1 and C_4 correspond to Fe chains adsorbed on the troughs of (1×5)Ir(100), whereas C_2 corresponds to Fe chains sitting on the hills of (1×5)Ir(100). DEC is the partially deconstructed structure, wherein the Fe atoms sit on the hollow sites of a quasisquare, locally deconstructed Ir(100). A and B indicate the Ir atoms nearest neighbors of Fe. Vertical displacements have been exaggerated for clarity purposes.

calculated in a grand-canonical definition, i.e., by subtracting the sum of the energy of the fully deconstructed structure and the energy of a bulk Ir atom to the energy of the reconstructed structure. However, the Ir surface deconstruction from (1×5) to (1×1) implies the removal of 20% of the first layer Ir atoms, which may not readily take place when the double chains are experimentally deposited at low temperature and low coverage.[10] At high T and/or high Fe coverages, full experimental deconstruction of Ir(100) takes place, with expulsion of the excess Ir atoms from the first layer and formation of Ir chains on top of the surface. Similar superstructures consisting of Ir rows on Ir(100) have recently been seen also in case of adsorption of H atoms on this surface at sufficiently high temperatures.[26] However, at low T and coverage, the (1×5) structure may be kinetically frozen, given the massive atomic migration and rearrangement required to produce the (1×1). A second possibility is a partial deconstruction of the surface, taking place without removal of any Ir atoms. A simple displacement of Ir atoms from beneath the Fe double chains (where the Ir layer structure may be locally altered) to beside the chains should be much less kinetically hindered than a full deconstruction. To investigate this possibility, we started from C_1 and C_4 structures and looked for concerted displacements of Fe and Ir atoms that would spontaneously lower the energy. The structures were perturbed by moving the Fe atoms midway between the C_1 and C_4 adsorption sites: then they were relaxed using a standard Broyden-Fletcher-Goldfarb-Shanno (BFGS) quasi-Newton method. It became apparent in this way that

TABLE IV. Coordinates of the DEC structure in the FM phase: only Fe atoms and Ir atoms belonging to the four uppermost layers are listed. The y axis is perpendicular to the surface, whereas the z axis is along the chains. In the NM and AFM DEC phases, positions of the Ir atoms do not differ appreciably from those in the FM phase.

Element	x (Å)	y (Å)	z (Å)	Element	x (Å)	y (Å)	z (Å)
Fe	9.537	13.424	1.365	Ir	1.379	9.686	1.374
Fe	7.015	13.424	1.367	Ir	11.055	7.823	−0.004
Ir	13.043	12.477	1.370	Ir	8.273	7.781	−0.003
Ir	8.274	11.664	2.747	Ir	5.492	7.823	−0.004
Ir	3.505	12.476	1.370	Ir	2.773	7.819	−0.004
Ir	10.948	11.700	−0.011	Ir	−0.015	7.819	−0.004
Ir	5.600	11.701	−0.010	Ir	12.413	5.852	1.376
Ir	1.379	11.905	−0.009	Ir	9.665	5.866	1.377
Ir	12.424	9.780	1.371	Ir	6.881	5.866	1.377
Ir	9.656	9.703	1.373	Ir	4.133	5.852	1.376
Ir	6.891	9.704	1.373	Ir	1.379	5.872	1.375
Ir	4.124	9.780	1.372				

both C_1 and C_4 structures are unstable against a lateral shifting motion of Ir atoms underneath the Fe chains. To lower the energy, the Ir atoms shifted sideways so as to restore a square ideal (100) geometry underneath the double chains and accumulating beside them. This Ir rearrangement yielded a partially deconstructed (1×5) structure wherein the Fe atoms sit on the hollow sites of a quasisquare, locally deconstructed Ir(100) surface (see Fig. 2, where the structure is denoted as DEC), slightly compressed along the direction perpendicular to the Fe chains (the Ir-Ir distance along this direction is 2.67 Å, to be compared to the equilibrium distance of 2.76 Å). The atomic coordinates of this structure in the FM phase are listed in Table IV. This structure is lowest in energy among the (1×5) Fe/Ir systems explored, with a large energy gain of about 0.46 eV per Fe atom with respect to C_4, which is the lowest energy reconstructed structure. Since STM images do not yield information on the position of Ir atoms beneath or besides the Fe chains, this partially deconstructed (1×5) Fe/Ir (DEC) structure seems as compatible as reconstructed (REC) C_1 and C_4 structures with available data and thus deserves to be investigated on similar grounds. We remark finally that *both* the REC and DEC surface geometries are strictly speaking metastable. We calculate in fact the total energy of double chains (coverage 0.4 ML) on a *completely deconstructed* Ir(100) surface to be still 0.11 eV /Fe atom lower than the energy of the DEC structure and 0.57 eV lower than that of the REC C_4 structure. The larger extent of the latter difference indicates however that most of the energy gains are obtained as soon as the Ir rearrangement is actuated locally beneath the Fe double chain, suggesting that structures such as DEC should be taken in serious consideration as structural candidates. The structural parameters for nonmagnetic, FM, and AFM wires on Ir(100) are shown in Table V. We note that, contrary to Ref. 12, and surprisingly given the similarity of approaches, the C_2 structure is highest in energy among all REC structures, rather than the lowest. We repeatedly checked all possible sources of error in our calculation but found none.

A. Ferromagnetism versus antiferromagnetism

In agreement with Ref. 12, we found for all structures that nonmagnetic configurations are always disfavored over the magnetic ones, reflecting Fe's strong Hund's rule coupling. We then considered in parallel the REC and DEC structures. In our calculations the lowest energy FM structure among the REC ones is C_1, whereas in Ref. 12 it was reported to be C_2, which is least favored in our calculations. In the AFM case, on the other hand, C_4 is lower in energy than either C_1 or C_2, although the structural energy difference between C_1 and C_4 is quite small, only 0.02 eV. C_2 is always the highest energy structure, which agrees with the experimental evidence that double chains appear to sit in the troughs of the (1×5)Ir(100).[10] However, the structural interchain distances of the C_1, C_4, and DEC structures are 2.42, 4.17, and 2.52 Å, respectively, all different from the apparent distances in the STM pictures, 3.3 ± 0.2 Å. As pointed out in Ref. 12, the error of this "experimental" value may well be much larger than 0.2 Å because apparent maxima in STM images may strongly deviate from actual centers of the Fe atoms. In conclusion, the STM pictures do not really discriminate between various structures. The calculated magnetic moments of Fe atoms are of the order of $3.1+/-0.1\mu_B$ in both FM and AFM configurations. The Ir atoms neighboring the magnetic Fe chains generally become magnetically polarized, with moments of order $0.1\mu_B-0.3\mu_B$ in the FM case; in the AFM case, on the other hand, some of the moments of nearby Ir atoms vanish by symmetry (in the DEC structure, they *all* vanish by symmetry).

We also considered AFM structures wherein Fe atoms transverse to the double chain have opposite magnetization signs (and the coupling between first neighbors parallel to the chain direction is still AFM). The energy of this transverse AFM configuration is higher than the longitudinal AFM one considered above by 0.04–0.1 eV per atom depending on the structure, with the exception of C_4, where the two configurations are practically degenerate. This is not un-

TABLE V. Calculated structural parameters and energetics for NM, FM, and AFM double chains on the (1×5)Ir(100) surface. C_1, C_2, and C_4 configurations, where the Ir surface is reconstructed (REC), are considered, as well as the structure where Fe chains sit on a partially deconstructed surface (DEC). The energy differences ΔE are given with respect to AFM DEC, which is the lowest energy configuration. In columns 3 and 4 the distances between Fe atoms and their nearest-neighbor Ir_A and Ir_B atoms (as indicated in Fig. 2) are provided. The interaction energy (E_{int}) for a given structure and magnetic configuration is defined as the difference between the total energy of the structure and the sum of the energies of the clean reconstructed (1×5)Ir(100) and twice the energy of the isolated Fe chain (with the same magnetic configuration).

		ΔE (eV)	Chain-chain d (Å)	Fe-Ir_A d (Å)	Fe-Ir_B d (Å)	m (μ_B)	E_{int} (eV)
C_1	NM	1.543	1.97	2.53	2.60	0.00	4.277
	FM	0.481	2.40	2.51	2.62	3.07	3.112
	AFM	0.480	2.42	2.49	2.59	3.06	3.254
C_2	NM	1.731	1.97	2.32	2.71	0.00	4.089
	FM	0.903	2.33	2.40	2.71	3.02	2.690
	AFM	0.895	2.31	2.38	2.70	2.99	2.840
C_4	NM	1.642	3.77	2.30	2.45	0.00	4.179
	FM	0.521	4.14	2.52	2.59	3.14	3.071
	AFM	0.459	4.17	2.49	2.55	3.15	3.275
DEC	NM	0.949	2.40	2.53	2.47	0.00	4.872
	FM	0.059	2.52	2.62	2.57	3.06	3.533
	AFM	0.000	2.57	2.58	2.55	3.02	3.734

expected for the distance between chains is large in C_4 so they weakly interact with each other. Since these transverse AFM structures are in general energetically higher than the longitudinal AFM ones, we will not investigate them further.

The demise of FM in favor of AFM in Ir-deposited chains is due to Fe-Ir hybridization, since free-standing double chains are always FM. Following a reasoning parallel to that of Kubetzka *et al.*[7] this could tentatively be rationalized in terms of changes in the respective FM and AFM susceptibilities. The FM susceptibility should be approximately proportional to the electronic DOS at the Fermi level evaluated in the NM state and projected on the Fe atoms, $n_{\text{Fe}}(E_F)$. We calculated the NM DOS for all the relevant structures and compared their projected value onto Fe atoms to the NM DOS of free-standing, coupled chains (see Figs. 3 and 4, where the NM projected DOS (PDOS) of the C_1 and the DEC structures are shown together with the FM and AFM ones; the PDOS of the C_2 and C_4 structures show a qualitatively similar behavior). Confirming expectations, we note a clear decrease of PDOS upon deposition on the Ir(100) surface. One might now be tempted to surmise that since $n_{\text{Fe}}(E_F)$ is reduced upon deposition on Ir(100) due to hybridization with Ir, ferromagnetism might be disfavored relative to AFM due to a selective decrease of the FM susceptibility relative to the AFM one. A PDOS decrease could reduce the violation of Stoner's FM criterion $1-Un(E_F)<0$ (where U is an exchange energy parameter), while the AFM susceptibility need not do exactly the same, as there is no straight *a priori* proportionality between PDOS and AFM susceptibility. To investigate that aspect, we conducted constrained magnetization calculations allowing a numerical evaluation of the zero-field FM and AFM susceptibilities. To reduce computational times, we did that for a "toy" DEC structure consisting of Fe atoms and nearest-neighbor Ir atoms only (in total 2+3 atoms in the FM cell and 4+6 atoms in the AFM cell). For this structure the AFM structure is lower in energy than the FM one by about 60 meV per Fe atom. The constraint on the Fe local magnetic moments (calculated by integrating the magnetization density in a sphere centered on the Fe atoms, as explained at the beginning of Sec. III) was imposed by adding a penalty functional to the total energy. As Fig. 5 shows, for small magnetizations there is a quadratic energy decrease with magnetization, which measures separately the FM and AFM susceptibilities. The FM and AFM energies remain however extremely close at all small magnetizations and do not indicate appreciable differences between FM and AFM susceptibilities. So while there is an Ir-induced FM susceptibility decrease connected with the Ir-induced decrease of $n_{\text{Fe}}(E_F)$, that does not seem to explain the switch from FM to AFM. The AFM energy gain is realized at large magnetization magnitudes, not revealed at the perturbative level.

The main notable Ir-related difference between FM and AFM states is the finite magnetic polarization required for the nearby Ir atoms in the FM case, contrasted by the symmetry-induced zero magnetic polarization for some (REC structures) or all (DEC structure) of the nearby Ir atoms in the AFM case. Due to an interplay between magnetism and structure, the Fe magnetic orbitals delocalize over the Ir substrate atoms in the FM case, but less, or not at all (depending on the structure), in the AFM case. As a result the Ir-related reduction of magnetic energy gain is less important in the AFM case than in the FM case. If this indeed is the mechanism that causes the switch from FM to AFM, then it could hold for other magnetic elements as well. To explore this hypothesis, we studied the magnetic properties of Mn,

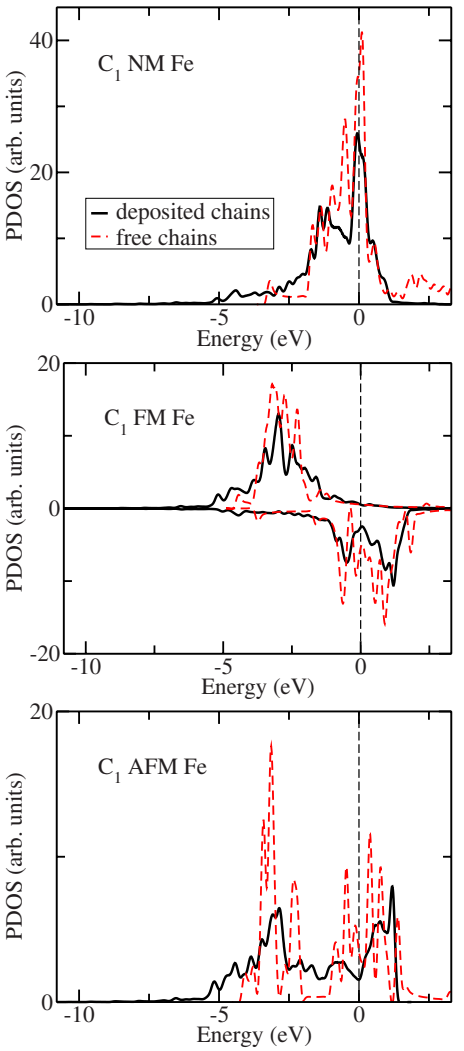

FIG. 3. (Color online) Ferromagnetic, antiferromagnetic, and nonmagnetic density of states of the C_1 REC structure projected onto Fe atoms. Dashed lines indicate the DOS of free-standing, double Fe wires. In the AFM case, the PDOS were calculated by projecting onto all of the Fe atoms, i.e., both those with positive magnetic moments and those with negative ones: as a consequence, the PDOS of spin-up and spin-down electrons are the same.

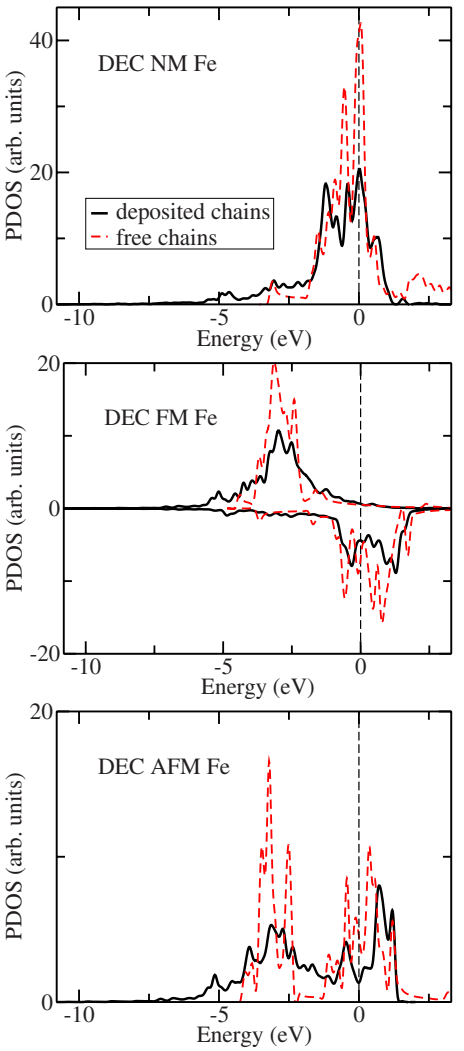

FIG. 4. (Color online) Ferromagnetic, antiferromagnetic, and nonmagnetic density of states of the partially deconstructed structure projected onto Fe atoms. Dashed lines indicate the DOS of free-standing, double Fe wires. In the AFM case, the PDOS were calculated by projecting onto all of the Fe atoms, i.e., both those with positive magnetic moments and those with negative ones: as a consequence, the PDOS of spin-up and spin-down electrons are the same.

Co, and Ni double chains on (1×5)Ir(100) (restricting to C_1 and DEC configurations). The starting unsupported Mn chains were found to be AFM, whereas Co and Ni chains were FM. Energy differences between FM and AFM Mn, Co, and Ni double chains [free standing and deposited on Ir(100)] are shown in Table VI, with Fe also shown by comparison. Similar to the Fe chains, the Ir surface was unstable against deconstruction when Mn, Co, or Ni chains are adsorbed on the surface. In the end, it turned out that Ir-deposited Co and Ni double chains were still FM, unlike Fe. However, the energy difference between FM and AFM structures was substantially reduced when Co and Ni chains were adsorbed on Ir(100) for all geometries (except for Co chains in C_1 geometry, where it increased by 0.03 eV). Double Mn chains remained AFM when deposited on Ir(100), but the energy gap between the AFM and FM configurations again increased. On the whole, these results seem to confirm our starting hypothesis. We may tentatively conclude therefore that the selective spill out of magnetization to Ir atoms near the Fe chains present in the FM state but reduced or absent in the AFM state should play an important role in shifting the energetic balance from FM toward AFM, although other subtler and more specific effects should be invoked in order to explain the dependence of the relative stability of FM and AFM configurations upon the transition-metal element and the adsorption structure. On this aspect there is room for further work addressing the physical mechanism in more detail, maybe resorting to some simplified and more transparent schemes such as tight binding.

B. Magnetic anisotropy

Magnetic anisotropy energies were calculated for both unsupported and deposited Fe double chains, where the REC

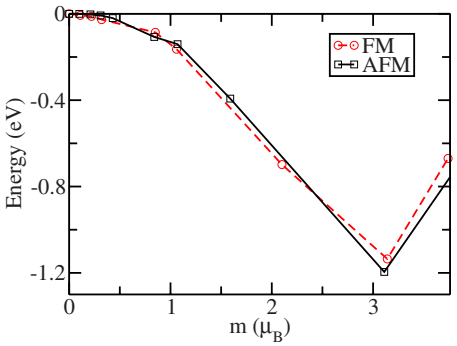

FIG. 5. (Color online) Total energy per Fe atom of "toy" DEC FM and AFM structures consisting of Fe atoms and nearest-neighbor Ir atoms as a function of the magnetic moment m on a Fe atom. These calculations were performed by adding a penalty functional to the total energy in order to constrain the local magnetic moment around a Fe atom. For small m, which corresponds to small magnetic fields and small staggered magnetic fields for the FM and AFM case, respectively, the dependence of the energy on m is quadratic and the coefficient of the quadratic term is inversely proportional to the FM or AFM susceptibility.

(C_1 and C_4) and the DEC configurations have been considered. In free AFM Fe double chains, the easy axis was found to lie along $\hat{y}$, perpendicular to the plane containing the chains for chain-chain distances corresponding to the C_1 and DEC structures (see Table VII). For large chain-chain distances, the easy axis switched to $\hat{z}$, along the chains, in agreement with the single chain limit.[27,28]

In Ir-deposited AFM Fe double chains the easy magnetization axis of both C_1 and C_4 REC structures was $\hat{x}$, parallel to the surface and perpendicular to the chains. In the DEC structure, $\hat{x}$ was instead the hard axis, whereas the easy axis was $\hat{z}$, parallel to the chains (see Table VII). These magnetic anisotropy results hold for FM configurations as well, as could be expected from phenomenological on-site anisotropy parameters. From the predicted opposite magnetic anisotropies of REC and DEC structures, it follows that the detection of the easy magnetization axis of the double chains on Ir(100) by SP-STM techniques could yield indirect but important information on the unknown local structure of the Ir(100) surface.

In principle, we note that magnetostatic effects due to magnetic dipolar interactions could also give rise to magnetic anisotropy effects. However, for our two-chain AFM system these dipole-dipole energies can be estimated to be less than 0.1 meV, much smaller than magnetocrystalline energies due to SOC, and can be neglected.

TABLE VII. Magnetic anisotropy energies (per atom) of unsupported FM single chains, unsupported double AFM Fe chains at d_{inter}=2.4 Å, and double AFM Fe chains deposited onto the Ir(100) surface for REC (C_1 and C_4) and DEC configurations. The intrachain Fe-Fe distance is 2.758 Å for all the structures. The z axis is along the chains, whereas the x axis is perpendicular to the chains and parallel to the plane containing the chains.

	E_z-E_x (10^{-3} eV)	E_z-E_y (10^{-3} eV)
Free FM single chain	1.9	1.9
Free AFM double chain (d_{inter}=2.4 Å)	0.5	−0.6
Dep. AFM double chain (C_1)	−0.7	0.6
Dep. AFM double chain (C_4)	−0.8	0.7
Dep. AFM double chain (DEC)	1.9	1.7

C. Dzyaloshinskii-Moriya interactions

The second important effect of spin-orbit interaction on magnetism is the onset of a Dzyaloshinskii-Moriya intersite interaction term of the form[29,30]

$$H_{\text{DM}} = \mathbf{D}_{ij} \cdot \mathbf{S}_i \times \mathbf{S}_j \quad (1)$$

where $\mathbf{D}_{ij}$ is the Dzyaloshinskii vector. The DM interaction is chiral and is due to the concerted effect of spin-orbit coupling and a lack of structural inversion symmetry at the surface. The direction of $\mathbf{D}_{ij}$ is determined solely by structural symmetry.[30] More specifically, the intrachain intersite $\mathbf{D}_{ij}$ must be orthogonal to a mirror plane containing sites R_i and R_j and parallel to a mirror plane bisecting R_{ij}. For the Fe double chains on Ir(100), where a pair of (magnetically parallel) Fe atoms is the effective magnetic site, the vector $\mathbf{D}_{ij}$ lies on the surface plane and normal to the double chain, i.e., parallel or antiparallel to the $\hat{x}$ axis. The sign of $\mathbf{D}_{ij}$, a vector which breaks the left-right structural symmetry, will switch by switching the sign of magnetization, in accordance with time-reversal symmetry. It is otherwise fully determined microscopically by the asymmetry of the self-consistent potential gradient in the surface region.

We calculated the magnitude and sign of $\mathbf{D}$, assumed to be restricted to first neighbors, by direct energy difference between two noncollinear magnetic structures of the deposited double chain, each composed of four Fe pairs or eight Fe atom/cell. The magnetization was constrained to be orthogonal between one Fe pair to the next down the double chain. In the first magnetic structure, the magnetization direction was taken to rotate in the sense $y,z,-y,-z$; in the second, it

TABLE VI. Energy difference (per adsorbed metal atom) between FM and AFM configurations of free-standing and deposited Mn, Fe, Co, and Ni double wires. C_1 and DEC configurations have been considered. Energies are in units of eV.

	Mn		Fe		Co		Ni	
	Free	Dep.	Free	Dep.	Free	Dep.	Free	Dep.
C_1	0.085	0.169	−0.092	0.001	−0.057	−0.088	−0.041	−0.012
DEC	0.090	0.143	−0.116	0.059	−0.098	−0.068	−0.045	−0.011

counter-rotated in the sense $y,-z,-y,z$. These two magnetic spirals have identical structural, exchange, and anisotropy energies, so that their energy difference identifies precisely the DM term alone.

Since heavy computational cost restricted us to relatively small systems, we considered two successive sizes, comprising, respectively, 12 and 36 Ir atoms, corresponding to Fe nearest-neighbor atoms and Fe nearest- and next-nearest-neighbor atoms, respectively. This allowed an appreciation of the kind of finite-size error involved, as well as some level of extrapolation toward ideally larger sizes. Atomic relaxations of the small systems were not taken into account, i.e., atoms were frozen at the positions obtained by relaxing the corresponding seven-layer slabs. Moreover, only two experimentally relevant structures were considered: the C_1 (REC) structure and DEC structure. (As discussed above, the distance between chains in C_4 is very large and somewhat less likely than C_1.)

It turns out that DM favors right-handed cycloidal spin spirals for both structures. As far as the REC structure is concerned, the magnitude D of the Dzyaloshinskii vector slightly increases for the larger size systems, from 2 to 3 meV, whereas anisotropy energies decrease somewhat from 3–4 meV to 1–2 meV. We conclude that for the REC deposited Fe double chain, MAEs are of the order of 1 meV (Table VII), whereas D is about 3 meV. In the DEC structure, both D and MAEs are large but do get significantly smaller in the larger size system: D drops from 12 to 7 meV and $K=K_z-K_y$ from 8 to 2 meV. Extrapolating, we conclude that in the DEC-deposited double chain the anisotropy energy K could be about 1 meV, D of order of 5 meV.

IV. ROTATING MAGNETISM VERSUS COLLINEAR ANTIFERROMAGNETISM

If anisotropy was ideally zero but at the same time the DM term was finite, no matter how small, the collinear AFM magnetic structure would spontaneously transform to a rotating magnetic structure, whose pitch would diverge as D tends to zero.[31] On the other hand, once anisotropy is large enough, the collinear AFM state will prevail over noncollinear magnetism. The relatively large anisotropies and DM values reported in the previous sections indicate that the competition between AFM and helical spin structures needs to be considered in quantitative detail, as was recently done for other systems by Blügel and co-workers.[32–34]

In the following we will describe our system by a micromagnetic continuous model:[35] for FM systems, this approximation is justified if the magnetic-moment variations are small on a length scale where exchange and DM interactions are significant. For our AFM double chains, given two intrachain nearest-neighbor sites i and $i+1$ with magnetizations $\mathbf{m}_i$ and $\mathbf{m}_{i+1}$, a micromagnetic model is valid if the difference between $\mathbf{m}_i$ and $-\mathbf{m}_{i+1}$ is small. Within this approximation, taking into account the quasi-one-dimensional nature of our systems, the energy functional is given by

$$E=\int_{-\infty}^{+\infty}\left[A\left(\frac{d\mathbf{m}}{dz}\right)^2+\bar{\mathbf{D}}\cdot\left(\mathbf{m}\times\frac{d\mathbf{m}}{dz}\right)+\mathbf{m}^{\dagger}\cdot\bar{\mathbf{K}}\cdot\mathbf{m}\right]dz, \tag{2}$$

where A is the spin stiffness, $\bar{\mathbf{D}}$ is an effective Dzyaloshinskii vector, and $\bar{\mathbf{K}}$ is an effective anisotropy energy tensor. Following the convention usually adopted in micromagnetic calculations, we assume that $m_x^2+m_y^2+m_z^2=1$. These three quantities depend on the crystal structure and can be expressed in terms of the exchange constants J_{ij}, $\mathbf{D}_{ij}$ vectors, and anisotropy energy tensor $\mathbf{K}$ of the discrete model. We may assume that only nearest-neighbor exchange and DM interactions are important. Then $A\sim d_{\text{intra}}J/2$, $\bar{\mathbf{D}}\sim\mathbf{D}$, and $\bar{\mathbf{K}}\sim\mathbf{K}/d_{\text{intra}}$, where d_{intra} is the Fe-Fe intrachain distance and J and $\mathbf{D}$ are the nearest-neighbor exchange and DM parameters. The nearest neighbor J is straightforwardly evaluated from the energy difference between FM and AFM phases.[36] In the following we will separately address two cases, namely:

(a) $\mathbf{D}=D\hat{x}$ parallel to the hard axis. This is the case in the DEC surface.

(b) $\mathbf{D}=D\hat{x}$ parallel to the easy axis. This is the case in the REC surface.

(a) If D is parallel to the hard axis, then the magnetic moments lie in the (y,z) plane, perpendicular to D, which contains the double chain and is orthogonal to the surface. In this case a collinear or two-dimensional noncollinear structure will appear, depending on the relative strength of D and the in-plane anisotropy parameter $K\equiv K_z-K_y$, where K_y and K_z are the $\hat{y}$ and $\hat{z}$ components of the anisotropy energy tensor. This problem is considered in detail in the literature[31,37] and excellently summarized in Ref. 38. For spin structures lying in the (y,z) plane, formula (2) simplifies to

$$E=\int_{-\infty}^{+\infty}\left[A\left(\frac{d\phi}{dz}\right)^2+\bar{D}\frac{d\phi}{dz}+\bar{K}\sin^2\phi\right]dz, \tag{3}$$

where ϕ is the angle between the local magnetization and the easy axis, $\hat{z}$, and $\bar{K}\equiv\bar{K}_y-\bar{K}_z$. A noncollinear, helical state will appear if the DM-related energy gain is higher than twice the formation energy of an optimal domain wall in the (y,z) plane.[31,37] This is equivalent to

$$D>\frac{4}{\pi}\sqrt{\frac{JK}{2}}. \tag{4}$$

Inserting the numerical values $J=29$ meV and $K=1.7$ meV, we obtain the inequality $D>6.3$ meV, estimated for the occurrence of a helical state in the DEC structure. From our calculations, we estimate D around 5 meV, smaller than the critical value, although generally of the same order of magnitude. Therefore, we tentatively conclude that the AFM collinear state is most likely in the DEC structure. In view of our poor accuracy, however, we cannot totally exclude a helical state with a very long pitch, consisting of wide antiferromagnetic domains separated by well-separated domain walls.

(b) if D is paralled to the easy axis, then three-dimensional noncollinear structures are also possible besides collinear and two-dimensional noncollinear ones. A thorough

description of this case can be found in Ref. 38. Since the condition $m_x^2+m_y^2+m_z^2=1$ holds, formula (2) can be written as

$$E=\int_{-\infty}^{+\infty}\left[A\left(\frac{d\mathbf{m}}{dz}\right)^2-\bar{D}\left(m_y\frac{dm_z}{dz}-m_z\frac{dm_y}{dz}\right)+(\bar{K}_y-\bar{K}_x)m_y^2+(\bar{K}_z-\bar{K}_x)m_z^2\right]dz, \quad (5)$$

where $\bar{K}_x$, $\bar{K}_z$, and $\bar{K}_y$ are the easy, intermediate, and hard components of the anisotropy energy tensor, respectively (see anisotropy energies for the C_1 REC structure in Table VII). Expanding the integrand of Eq. (5) around the AFM solution, $m_y=m_z=0$, one gets the following Euler-Lagrange equations:

$$A\frac{d^2m_y}{dz^2}+\bar{D}\frac{dm_z}{dz}-(\bar{K}_y-\bar{K}_x)m_y=0, \quad (6)$$

$$A\frac{d^2m_z}{dz^2}-\bar{D}\frac{dm_y}{dz}-(\bar{K}_z-\bar{K}_x)m_z=0. \quad (7)$$

Considering again only nearest-neighbor J and $\mathbf{D}$, these equations have a periodic solution

$$m_y=\alpha_y\cos(\omega z+\beta_y), \quad (8)$$

$$m_z=\alpha_z\cos(\omega z+\beta_z), \quad (9)$$

if and only if[38]

$$D>\sqrt{\frac{J}{2}(K_z-K_x)}+1. \quad (10)$$

Moreover, when the above inequality is fulfilled, the noncollinear state is always lower in energy than the AFM collinear solution. Therefore, when $D=\sqrt{\frac{J}{2}(K_z-K_x)}+1$, a second-order phase transition to a three-dimensional state takes place. The system undergoes a second-order transition to a two-dimensional helical state in the (y,z) plane at slightly higher values of D, but this critical point cannot be determined analytically.[38] We should emphasize that, in our case, the range of D values where the three-dimensional state is stable (which depends on the magnitude of the components of the magnetic anisotropy tensor, see Ref. 38) is very narrow. Inserting the numerical values $J=0.5$ meV and $K_z-K_x=0.7$ meV corresponding to C_1 in formula (10), we obtain that the AFM will be destabilized if $D>1.4$ meV. Since our REC surface calculations suggest D values around 3 meV, which is larger than this threshold, we conclude that in a REC structure such as C_1, where the double chains do not deconstruct the underlying Ir(100) surface, the magnetic ground state should be noncollinear and in particular a (y,z) helical state is the most likely outcome. In conclusion, a sketch of the predicted magnetic ground state for the DEC and REC (C_1) structures is shown in Fig. 6.

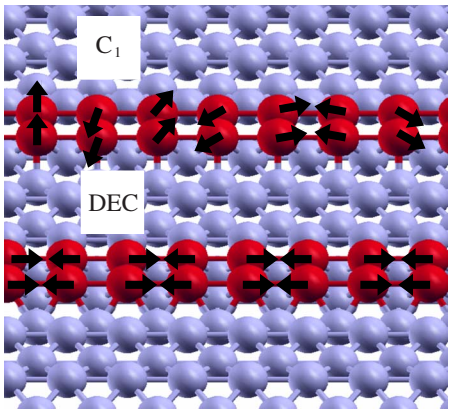

FIG. 6. (Color online) View of the spin-structure of the reconstructed C_1 and the partially deconstructed DEC Ir(100) configuration: Fe magnetic moments in C_1 are expected to form a right-handed cycloidal spin spiral, whereas in DEC a collinear AFM state with moments parallel to the chains should prevail.

V. DISCUSSION AND CONCLUSIONS

We studied by *ab initio* electronic structure and total-energy calculations Fe double chains on (1×5)Ir(100). Several different structures with the experimentally observed (1×5) periodicity were considered, particularly one, C_1 REC, where the underlying Ir surface remains quasihexagonally reconstructed, and another, DEC, where it is partially deconstructed, with a large decrease of total energy. By addressing magnetism first without spin-orbit effects, we find that in all structures considered the deposited Fe double chains do not remain FM as in vacuum, but generally adopt an AFM ground state. The demise of ferromagnetism is attributed to Fe-Ir hybridization. The hybridization of Fe with the Ir substrate brings about first of all a drop of the Fe-projected density of electronic states near E_F in the nonmagnetic state, which reduces the FM susceptibility. However, we find that the AFM susceptibility is also reduced by the same amount upon adsorption. At large magnetization, AFM appears eventually to be favored by a magnetization node intervening by symmetry in the bridging Ir atoms, a node which is absent in the FM case. By including spin orbit in the calculations, the magnetic anisotropy energies of relevant REC and DEC structures have been determined. The easy axis is found to lie in the surface plane and perpendicular to the Fe double chain in the REC structure, and parallel to the chains in the DEC structure. Finally, we calculated the Dzyaloshinskii-Moriya spin-spin interaction energy and found it to be generally of a competitive magnitude when compared to anisotropy. The different possibilities arising for the resulting ground-state magnetization pattern are examined. Within the substantial uncertainties connected with our estimated computational and finite-size errors, we conclude that a collinear AFM state with in-plane magnetization vector is likely to prevail in the DEC structure, whereas a long-period rotating magnetization in an orthogonal plane could instead prevail in the REC structure. These predictions and clear signatures should be of value for future experimental observations by SP-STM techniques.

ACKNOWLEDGMENTS

We are grateful to R. Wiesendanger for providing the initial motivation to conduct this study. We warmly acknowledge many instructive discussions with, and much help by, Andrea Dal Corso. Discussions with S. Blügel and R. Gebauer were also stimulating. The work was directly sponsored by MIUR PRIN/Cofin under Contract No. 2006022847 as well as by INFM/CNR "Iniziativa transversale calcolo parallelo." The research environment provided by the independent ESF project CNR-FANAS-AFRI was also very useful. Parts of the calculations were carried out on the SP5 machine at CINECA, Casalecchio.

*Corresponding author. Present address: Department of Chemistry and Applied Biosciences, Computational Science, ETH Zurich, USI Campus, via Giuseppe Buffi 13, CH-6900 Lugano, Switzerland; riccardo.mazzarello@phys.chem.ethz.ch

[1] S. C. Abrahams, L. Guttman, and J. S. Kasper, Phys. Rev. **127**, 2052 (1962).
[2] U. Gonser, C. J. Meechan, A. H. Muir, and H. Wiedersich, J. Appl. Phys. **34**, 2373 (1963).
[3] Y. Tsunoda, J. Phys.: Condens. Matter **1**, 10427 (1989).
[4] D. Li, M. Freitag, J. Pearson, Z. Q. Qiu, and S. D. Bader, Phys. Rev. Lett. **72**, 3112 (1994).
[5] D. Qian, X. F. Jin, J. Barthel, M. Klaua, and J. Kirschner, Phys. Rev. Lett. **87**, 227204 (2001).
[6] R. Wiesendanger, H.-J. Güntherodt, G. Güntherodt, R. J. Gambino, and R. Ruf, Phys. Rev. Lett. **65**, 247 (1990).
[7] A. Kubetzka, P. Ferriani, M. Bode, S. Heinze, G. Bihlmayer, K. von Bergmann, O. Pietzsch, S. Blügel, and R. Wiesendanger, Phys. Rev. Lett. **94**, 087204 (2005).
[8] H. J. Elmers and U. Gradmann, Appl. Phys. A: Solids Surf. **51**, 255 (1990).
[9] K. von Bergmann, S. Heinze, M. Bode, E. Y. Vedmedenko, G. Bihlmayer, S. Blügel, and R. Wiesendanger, Phys. Rev. Lett. **96**, 167203 (2006).
[10] L. Hammer, W. Meier, A. Schmidt, and K. Heinz, Phys. Rev. B **67**, 125422 (2003).
[11] R. Wiesendanger, private communication.
[12] D. Spišák and J. Hafner, Surf. Sci. **546**, 27 (2003).
[13] J. P. Perdew, K. Burke, and M. Ernzerhof, Phys. Rev. Lett. **77**, 3865 (1996).
[14] S. Baroni, A. Dal Corso, S. de Gironcoli, and P. Giannozzi, http://www.quantum-espresso.org
[15] Some of the effects involving small spin-orbit related energies were obtained and checked independently for accuracy using perturbation theory.
[16] A. M. Rappe, K. M. Rabe, E. Kaxiras, and J. D. Joannopoulos, Phys. Rev. B **41**, 1227 (1990).
[17] J. Monkhorst and J. D. Pack, Phys. Rev. B **13**, 5188 (1976).
[18] M. Methfessel and A. T. Paxton, Phys. Rev. B **40**, 3616 (1989).
[19] D. Spišák and J. Hafner, Phys. Rev. B **65**, 235405 (2002).
[20] T. Nautiyal, T. H. Rho, and K. S. Kim, Phys. Rev. B **69**, 193404 (2004).
[21] J. C. Tung and G. Y. Guo, Phys. Rev. B **76**, 094413 (2007).
[22] F. R. De Boer, R. Boom, W. C. M. Mattens, M. A. R. Niessen, and A. K. Niessen, *Cohesion in Metals* (North-Holland, Amsterdam, 1998).
[23] T. N. Rhodin and G. Brodén, Surf. Sci. **60**, 466 (1976).
[24] Q. Ge, D. A. King, N. Marzari, and M. C. Payne, Surf. Sci. **418**, 529 (1998).
[25] N. Bickel and K. Heinz, Surf. Sci. **163**, 435 (1985); K. Johnson, Q. Ge, S. Titmuss, and D. A. King, J. Chem. Phys. **112**, 10460 (2000); A. Schmidt, W. Meier, L. Hammer, and K. Heinz, J. Phys.: Condens. Matter **14**, 12353 (2002).
[26] L. Hammer, W. Meier, A. Klein, P. Landfried, A. Schmidt, and K. Heinz, Phys. Rev. Lett. **91**, 156101 (2003).
[27] G. Autes, C. Barreteau, D. Spanjaard, and M.-J. Desjonqueres, J. Phys.: Condens. Matter **18**, 6785 (2006).
[28] Y. Mokrousov, G. Bihlmayer, S. Heinze, and S. Blügel, Phys. Rev. Lett. **96**, 147201 (2006).
[29] I. E. Dzyaloshinskii, Sov. Phys. JETP **5**, 1259 (1957).
[30] T. Moriya, Phys. Rev. **120**, 91 (1960).
[31] Yu. A. Izyumov, Sov. Phys. Usp. **27**, 845 (1984); Usp. Fiz. Nauk **144**, 439 (1984).
[32] M. Bode, M. Heide, K. von Bergmann, P. Ferriani, S. Heinze, G. Bihlmayer, A. Kubetzka, O. Pietzsch, S. Blügel, and R. Wiesendanger, Nature (London) **447**, 190 (2007).
[33] P. Ferriani, K. von Bergmann, E. Y. Vedmedenko, S. Heinze, M. Bode, M. Heide, G. Bihlmayer, S. Blügel, and R. Wiesendanger, Phys. Rev. Lett. **101**, 027201 (2008).
[34] M. Heide, G. Bihlmayer, and S. Blügel, Phys. Rev. B **78**, 140403(R) (2008).
[35] W. F. Brown, *Micromagnetics* (Wiley, New York, 1963).
[36] It should be noted that the value of J is very small, especially in the C_1 REC structure. The reason why AFM competes with and narrowly wins over with FM is discussed earlier in the paper. Our tentative conclusion is that it is related to the unfavorable circumstance that a bridging Ir atom must acquire a spin polarization in the FM state, whereas spin polarization has a node at that atom in the AFM state. Of course with J values in the meV range there can be no order, even of the Kosterlitz-Thouless type, unless temperature is hundreds of milliKelvin—which however is where spin-polarized STM experiments are usually performed.
[37] I. E. Dzyaloshinskii, Sov. Phys. JETP **20**, 665 (1965).
[38] M. Heide, Ph.D. thesis, RWTH-Aachen, 2006.